Article

Cell Metabolism

Glycolysis-Mediated Changes in Acetyl-CoA and Histone Acetylation Control the Early Differentiation of Embryonic Stem Cells

Graphical Abstract

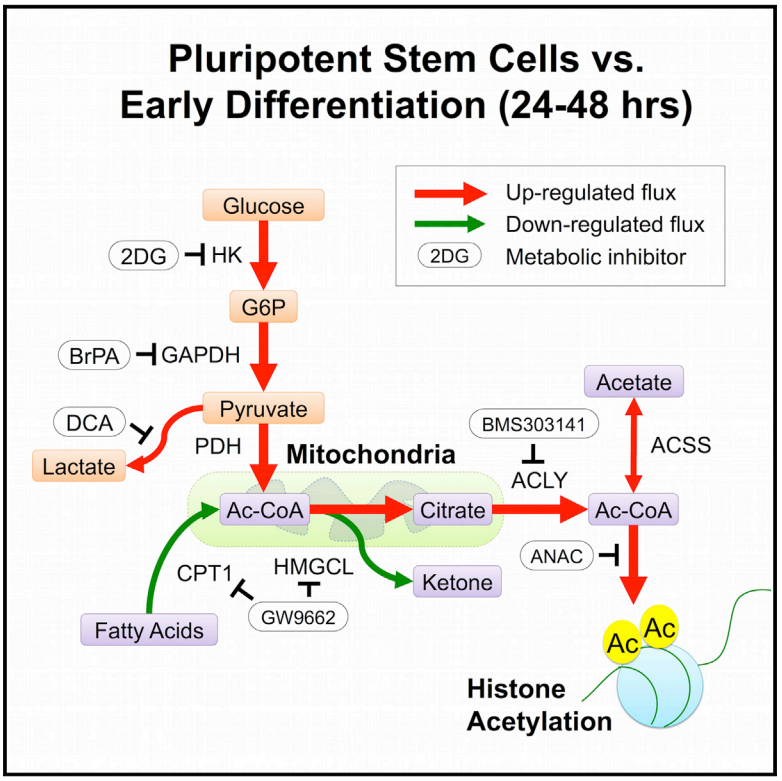

Highlights

- The metabolic profile of embryonic stem cell changes within hours of differentiation
- Glycolytic production of acetyl-CoA promotes histone acetylation during pluripotency
- Glycolysis inhibition leads to deacetylation and differentiation of pluripotent cells
- Pharmacologic modulation of acetyl-CoA regulates pluripotency

Authors

Arieh Moussaieff, Matthieu Rouleau, ..., Daniel Aberdam, Yaakov Nahmias

Correspondence

ariehm@ekmd.huji.ac.il (A.M.), ynahmias@cs.huji.ac.il (Y.N.)

In Brief

Moussaieff et al. show that the initial induction of human and mouse pluripotent stem cell differentiation is accompanied by a reduction of glycolysis-generated acetyl-CoA, which affects histone acetylation. Inhibition of glycolysis or acetyl-CoA led to differentiation of embryonic stem cells. See also associated Preview by Daley.

Moussaieff et al., 2015, Cell Metabolism *21*, 392–402
March 3, 2015
http://dx.doi.org/10.1016/j.cmet.2015.02.002

CellPress

CellPress

Cell Metabolism
Article

Glycolysis-Mediated Changes in Acetyl-CoA and Histone Acetylation Control the Early Differentiation of Embryonic Stem Cells

Arieh Moussaieff,[1,2,3,4,5,*] Matthieu Rouleau,[6,7] Daniel Kitsberg,[1,2] Merav Cohen,[1,2] Gahl Levy,[1] Dinorah Barasch,[5] Alina Nemirovski,[5] Shai Shen-Orr,[8] Ilana Laevsky,[8] Michal Amit,[8] David Bomze,[1,2] Bénédicte Elena-Herrmann,[9] Tali Scherf,[10] Malka Nissim-Rafinia,[2,11] Stefan Kempa,[12] Joseph Itskovitz-Eldor,[8] Eran Meshorer,[2,11] Daniel Aberdam,[3,4,13] and Yaakov Nahmias[1,2,13,*]

[1]Grass Center for Bioengineering, Hebrew University of Jerusalem, Jerusalem 9190401, Israel
[2]Alexander Silberman Institute of Life Sciences, Hebrew University of Jerusalem, Jerusalem 9190401, Israel
[3]INSERM, U976, Paris 75205, France
[4]Université Paris-Diderot, Paris 75205, France
[5]Institute for Drug Research, Hebrew University of Jerusalem, Jerusalem 91120, Israel
[6]Laboratoire de Physio-Médecine Moléculaire, CNRS UMR7370, Nice 06107, France
[7]Université de Nice Sophia Antipolis, Nice 06100, France
[8]Faculty of Medicine, Technion, Haifa 31096, Israel
[9]Centre de RMN à Très Hauts Champs, Institut des Sciences Analytiques, CNRS/ENS Lyon/UCB Lyon 1, Lyon 69100, France
[10]Weizmann Institute of Science, Rehovot 76100, Israel
[11]The Edmond and Lily Safra Center for Brain Sciences, The Hebrew University of Jerusalem, Jerusalem 91904, Israel
[12]The Max Delbrück Center for Molecular Medicine, Berlin 13125, Germany
[13]Co-senior author
*Correspondence: ariehm@ekmd.huji.ac.il (A.M.), ynahmias@cs.huji.ac.il (Y.N.)
http://dx.doi.org/10.1016/j.cmet.2015.02.002

SUMMARY

Loss of pluripotency is a gradual event whose initiating factors are largely unknown. Here we report the earliest metabolic changes induced during the first hours of differentiation. High-resolution NMR identified 44 metabolites and a distinct metabolic transition occurring during early differentiation. Metabolic and transcriptional analyses showed that pluripotent cells produced acetyl-CoA through glycolysis and rapidly lost this function during differentiation. Importantly, modulation of glycolysis blocked histone deacetylation and differentiation in human and mouse embryonic stem cells. Acetate, a precursor of acetyl-CoA, delayed differentiation and blocked early histone deacetylation in a dose-dependent manner. Inhibitors upstream of acetyl-CoA caused differentiation of pluripotent cells, while those downstream delayed differentiation. Our results show a metabolic switch causing a loss of histone acetylation and pluripotent state during the first hours of differentiation. Our data highlight the important role metabolism plays in pluripotency and suggest that a glycolytic switch controlling histone acetylation can release stem cells from pluripotency.

INTRODUCTION

Pluripotent stem cells (PSCs) are defined by their self-renewal and the ability to differentiate into all adult cell types (Blair et al., 2011). Supported by growth factors such as bFGF, the pluripotent state is defined by a handful of transcription factors, including OCT4, SOX2, and NANOG. The loss of the pluripotent state is a relatively slow process, leading over days to the gradual acquisition of a different transcriptional state. Importantly, the earliest events initiating this loss of pluripotency during the first steps of differentiation are largely unknown.

Metabolic processes are leading candidates for regulating this transition, as chemical fluxes change within minutes and can affect both transcriptional and epigenetic mechanisms. In fact, the metabolic profile of PSCs was found to be different from that of their terminally differentiated somatic counterparts (Cezar et al., 2007; Folmes et al., 2011; Meissen et al., 2012; Panopoulos et al., 2012; Shyh-Chang et al., 2013; Yanes et al., 2010). PSC metabolism showed the Warburg effect, a shift from oxidative phosphorylation to aerobic glycolysis characteristic of cancer cells (Folmes et al., 2011; Panopoulos et al., 2012; Zhu et al., 2010). This increase in glycolysis generates ATP at a faster rate than oxidative phosphorylation, while producing less reactive oxygen species (ROS), an important feature for rapidly proliferating cells. Glycolysis also shunts into the pentose phosphate pathway, producing much-needed nucleotides for proliferation (Vander Heiden et al., 2009).

In fact, glycolysis has recently been shown to increase reprograming efficiency of human and mouse fibroblasts (Folmes et al., 2011; Zhu et al., 2010). PS48, a PDK1 activator that blocks the entrance of pyruvate to the mitochondria, enhanced reprogramming efficiency (Zhu et al., 2010), while DCA, a PDK1 inhibitor, significantly reduced reprogramming (Folmes et al., 2011). Interestingly, both acetate and acetyl-CoA (Ac-CoA) were found to be elevated in metabolic profiles of PSCs at the end of differentiation process. However, the dynamics of this metabolic change are unclear. Importantly, although Ac-CoA is a cornerstone of

both carbohydrate and lipid metabolism, its origin and role in regulating stem cell pluripotency are largely unknown.

Recently, Shyh-Chang and colleagues demonstrated that threonine metabolism led to accumulation of Ac-CoA in mouse embryonic stem cells (mESCs), fueling synthesis of S-adenosylmethionine (SAM) for histone methylation (Shyh-Chang et al., 2013). In addition, earlier work showed the role of ATP-citrate lyse (ACLY) in producing Ac-CoA for histone acetylation of somatic cells (Wellen et al., 2009).

In this work, we sought to identify the earliest metabolic changes induced during the first hours of spontaneous differentiation. High-resolution nuclear magnetic resonance (NMR) analyses identified 44 metabolites, showing a gradual transition in metabolism over the first 48 hr of spontaneous differentiation. Surprisingly, glycolysis was driven toward production of Ac-CoA and acetate in PSCs, in addition to lactate. Moreover, acetate stimulation blocked early histone deacetylation, delaying loss of pluripotency and differentiation. We show that glycolytic inhibitors upstream of acetate caused the differentiation of PSCs, while those downstream of acetate delayed the exit from pluripotency. Our data suggest that a rapid loss of glycolysis in early differentiation downregulates Ac-CoA and acetate production, causing loss of histone acetylation and associated loss of pluripotency. It highlights a critical role for metabolism in the maintenance of chromatin at the pluripotent state, suggesting that a glycolytic switch triggers the loss of pluripotency during the earliest steps of differentiation.

RESULTS

The Metabolic Profile of hPSCs Changes during Early Differentiation

To study the earliest metabolic changes during the first steps of differentiation, we cultured I3 and I4 human embryonic stem cells (hESCs) in suspension (Figure 1A) (Amit et al., 2011) and removed bFGF from the medium for unbiased spontaneous differentiation. No significant changes were noted in the expression of the pluripotency markers *OCT4*, *NANOG*, or *REX1* during the first 48 hr of differentiation (Figure 1B), but changes in early-specification genes *PAX6* and *Brachyury* indicated early differentiation (Figure 1C). Despite the mild changes in gene expression, partial least-squares discriminant analysis (PLS-DA) of NMR spectral bins demonstrated significant changes in the metabolic profile of hESC media (Figure 1D; Figures S1A and S1B; $p < 0.001$ by permutation test) and extracts (Figure 1E; $p = 0.019$ by permutation test) as early as 24 hr into differentiation. This metabolic shift was further corroborated by hierarchical clustering analysis (Figure 1F). Altogether, 44 metabolites were identified (Figure S1C), constructing the first metabolic profile of PSCs during early differentiation, as well as the first comprehensive dataset of the metabolome of hESC cultivated in suspension as far as we know. Loading plots of extracellular and intracellular metabolites (Figure 1G) showed that lactate, acetate, and phosphocholine levels discriminated pluripotent from early-differentiated cells. The abundance of lactate and acetate was higher in I4 and I3 hESC samples and dropped during early differentiation (Figure 1H). To focus our analysis on metabolic pathways that affect differentiation, we exposed differentiating hESCs to the discriminatory metabolites identified above. Acetate addition significantly delayed the loss of pluripotency marker SSEA4 (Figure 1I), suggesting that this metabolite may be involved in cell exit of pluripotency.

Rapid Loss of Glycolysis-Produced Ac-CoA during Early Differentiation

Acetate is produced from Ac-CoA, a common building block of lipids and an endpoint of glycolysis. Indeed, we show a 2-fold higher concentration of Ac-CoA in pluripotent cells compared to early-differentiating cells ($p \leq 0.01$; Figure 2A). Interestingly, pluripotent cells show little uptake of fatty acids or cholesterol (Figures 2B–2D), suggesting that Ac-CoA production is primarily driven by an increased rate of glycolysis that is 2–3 orders of magnitude higher (Figures 2E and 2F). Indeed, metabolic flux tracing shows a 3-fold higher ^{13}C Ac-CoA production in pluripotent cells compared to early differentiation following *D-Glucose-*$^{13}C_6$ feeding (Figure 2G).

Quantitative gene expression analysis shows 2-, 5-, and 4-fold lower expression of *pyruvate dehydrogenase* (*PDH*) complex genes, *ACLY*, and *acetyl-coenzyme A synthetase* (*ACCS2*), respectively, after 48 hr of spontaneous differentiation (Figure 2H). No significant change was noted in the expression of *CPT1A*, an essential step in the β-oxidation of long-chain fatty acids. Importantly, while stimulation of differentiating cells with acetate increased Ac-CoA levels ($p \leq 0.05$), it did not affect glycolysis (Figures 2E and 2F) or the expression of *ACSS2*, hence meeting the cellular requirements for Ac-CoA. Proteomic analysis confirmed these findings, showing downregulation of ACLY and ACSS2, but little change in PDHA1 and PDHB (Figure S2A). Proteome analysis also suggested a downregulation of the monocarboxylate transporter SLC16A1, carrying short-chain fatty acids with one carboxylate group. Altogether, these data demonstrate that pluripotent cells direct glycolysis toward the production of Ac-CoA in addition to lactate, in contrast to the classic portrayal of the Warburg effect (Figure 2I).

Acetate Stimulation Delays Early Differentiation of Human and Mouse ESCs

Acetate was previously shown to accumulate during reprogramming of mouse induced pluripotent stem cells (iPSCs) (Folmes et al., 2011), but its modulation failed to enhance reprogramming efficiency. To characterize the effect of acetate on differentiation, we tested the expression of the pluripotency markers Tra-1-60 and Tra-1-81 in I3 hESCs following 4 days of differentiation in suspension and found a significant delay in the downregulation of both pluripotency markers (Figures 3A and 3B). To validate this effect across different cell lines, platforms, and species, we supplemented the media of H1 *OCT4-GFP* and mouse R1 *OCT4-GFP* cells with acetate. Acetate blocked OCT4 loss after 4 days of spontaneous differentiation (Figures 3C and 3D) as well as the change in colony morphology in R1 cells (Figure 3E). Cell number was similar for all conditions, suggesting acetate treatment had no significant effect on proliferation (Figure 3F). We next asked whether acetate could also block directed differentiation. H1 hESCs were induced toward endoderm using activin-A and Wnt3A, resulting in 15% SOX17-positive cells after 24 hr (Figure 3G). The addition of acetate blocked endodermal induction, with fewer than than 2.5% of the cells being positive for SOX17 ($p < 0.001$).

To study the dynamics of the effect of acetate on pluripotency, we introduced acetate to hESC medium either 24 or 48 hr after

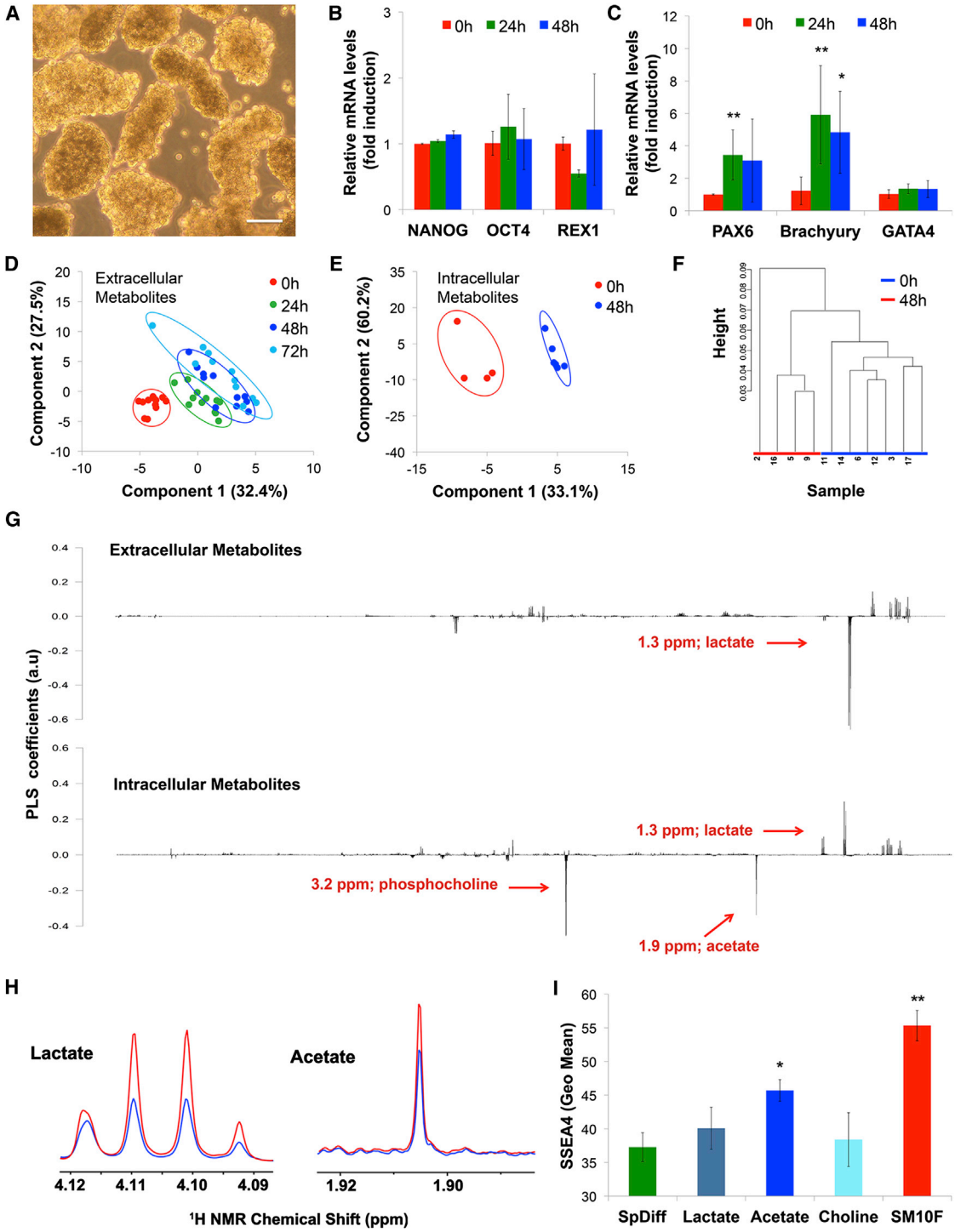

Figure 1. Metabolic Signatures of Early Differentiation

(A) Phase image of hESCs expanded and differentiated in high-density suspension culture. Bar, 100 μm.

(B) qRT-PCR analysis shows no significant changes in the expression of the pluripotency markers *NANOG*, *OCT4*, and *REX1* during the first 48 hr of differentiation.

(C) Early-differentiation markers *PAX6* and *Brachyury* show minor but significant increase in expression over the same time period.

(D–F) High-resolution NMR unveils significant changes in extracellular metabolites during the first 24 hr of spontaneous differentiation, as determined by multivariate tests of NMR spectra bins. (D) Partial least-squares discriminant analysis (PLS-DA) of ^{1}H-NMR spectral bins of extracellular metabolites shows significant changes after 24 hr of differentiation ($p < 0.001$; n = 10–12) and a clear gradient of metabolic change over the first 72 hr. (E) PLS-DA of intracellular metabolites shows significant differences as well ($p \leq 0.05$; n = 4–6). (F) Hierarchical clustering separates NMR spectra bins of cell extracts at 0 and 48 hr.

(legend continued on next page)

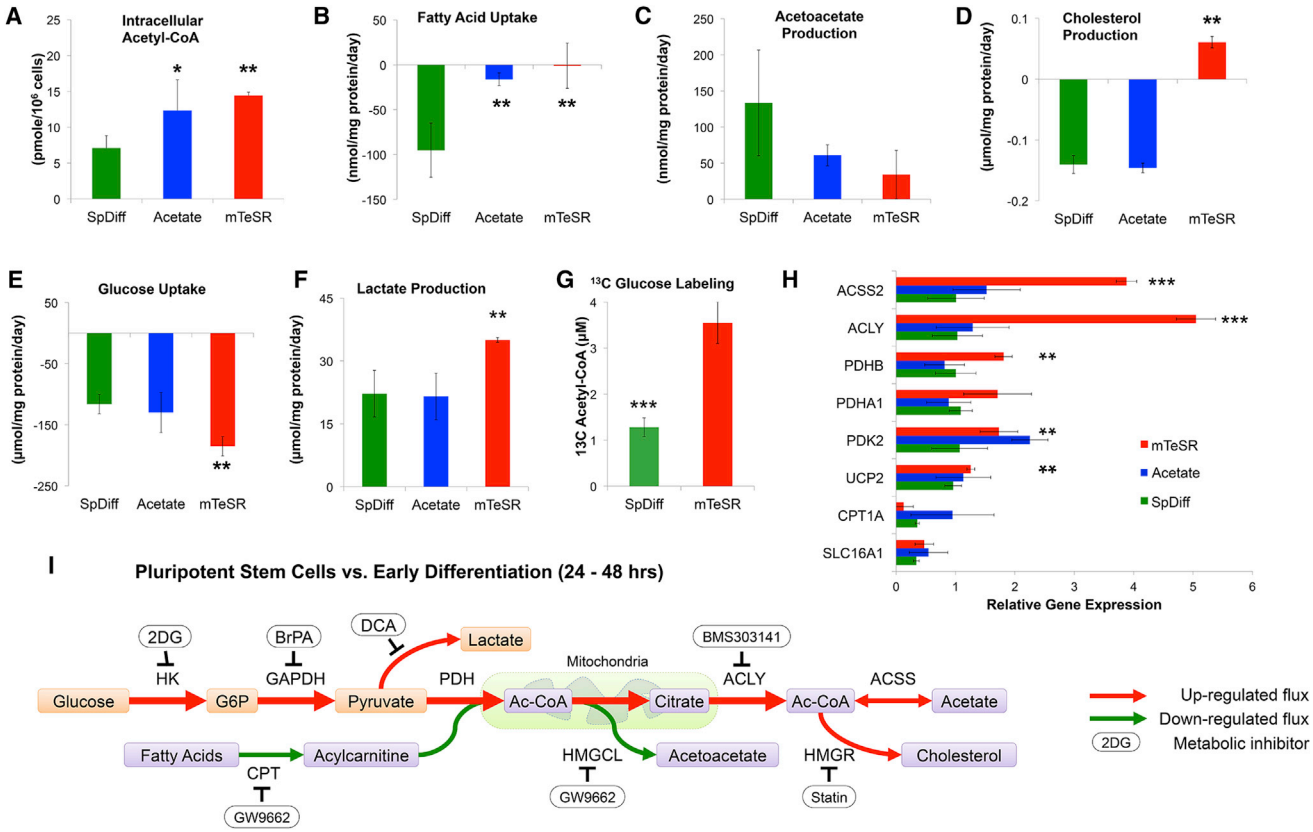

Figure 2. Rapid Loss of Glycolysis Produced Ac-CoA during Differentiation

(A–F) Targeted metabolomics corroborated significant changes in energy metabolism in H1 cells already at 24 hr of spontaneous differentiation. (A) Ac-CoA production was significantly higher in mTeSR than in SpDiff medium. Upon addition of acetate (10 mM) to SpDiff medium, Ac-CoA levels were increased to the levels found in mTeSR. (B and C) Fatty acid consumption and the production of ketone bodies by hESCs is minor, but upregulated in early-differentiating cells. (D) Cholesterol is released from H1 cells in mTeSR medium and consumed in SpDiff medium with or without acetate. (E and F) Higher consumption of glucose and production of lactate by hESCs, as expected in aerobic glycolysis.

(G) ^{13}C Ac-CoA levels were significantly decreased in early-differentiating hESCs following incubation with ^{13}C glucose.

(H) The expression of *ACSS2*, *PDK2*, *PDHB*, and *ACLY*, responsible for the formation of Ac-CoA, is significantly decreased during early spontaneous differentiation (SpDiff). *UCP2* levels showed only mild, although significant, change, and the expression of *PDHA1*, *CPT1A*, and *SLC16A1* showed no significant change.

(I) Glycolytic flux decreases upon early differentiation, redirecting from the formation of lactate and Ac-CoA to oxidative phosphorylation.

Error bars represent standard deviation. *p ≤ 0.05; **p ≤ 0.01; ***p ≤ 0.001.

induction of differentiation. Figure 3H shows that in both cases acetate could still block the loss of OCT4 expression and even rescue the pluripotent phenotype. We then added acetate to hESCs cultivated with bFGF, without feeder cells. Acetate delayed the spontaneous loss of OCT4 in H1 cells after 5 days of culture (Figure 3I), suggesting that acetate could complement bFGF in maintaining pluripotency. This effect was still efficient even after eight passages (Figures S3A and S3B). Finally, we tested the effect of different concentrations of acetate on pluripotency. Acetate significantly and dose-dependently inhibited loss of *Tra1-81*$^+$/*OCT4*$^+$ pluripotent cells in this model (Figures 3J and 3K). While the addition of 1 mM of acetate exerted a highly significant increase in the percentage of pluripotent cells, addition of citrate showed no effect (Figure S2C).

Acetate Increases Histone Acetylation in ESCs

Histone acetylation plays a critical role in the maintenance of PSC open chromatin structure (Hezroni et al., 2011; Melcer

(G) PLS-DA loadings reveal lactate was an influential metabolite in the separation of extracellular metabolites (top), while lactate, acetate, and phosphocholine were the discriminating metabolites in cell extract analysis (bottom).

(H) NMR peaks of secreted lactate (0 versus 48 hr) and intracellular acetate showing decrease of both at early-differentiating (blue) when compared to undifferentiated (red) hESCs.

(I) FACS analysis of SSEA4 in I4 hESCs cultured in SM10F medium compared to cells cultured in spontaneous differentiation medium (SpDiff) supplemented with lactate, acetate, or choline (10 mM each). Acetate supplementation significantly delayed loss of SSEA4 expression. Error bars represent standard deviation. *p ≤ 0.05; **p ≤ 0.01.

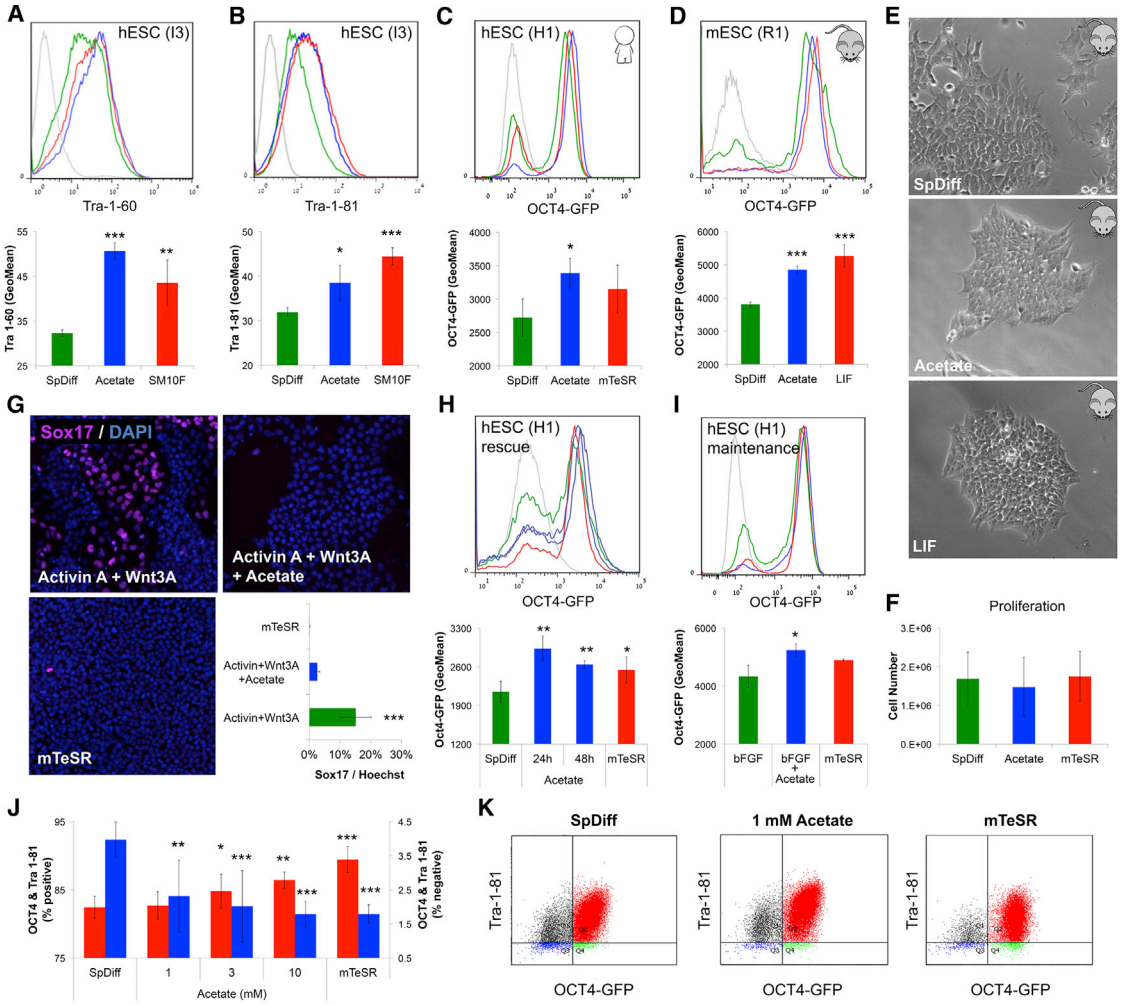

Figure 3. Acetate Delays Early Differentiation

(A and B) FACS analyses of I3 hESCs differentiated in suspension for 4 days. Spontaneous differentiation (SpDiff) led to a significant loss of the pluripotency markers Tra-1-60 and Tra-1-81 compared to cells cultured in SM10F medium, while the addition of 10 mM acetate blocked this change.

(C and D) FACS analyses of H1 hESCs and R1 mESCs expressing *OCT4-GFP* show that 10 mM acetate significantly inhibited loss of OCT4 expression after 4 days of spontaneous differentiation.

(E) Phase images of R1 mESCs show a rapid loss of pluripotent morphology during spontaneous differentiation (SpDiff), an effect that is negated by the addition of 10 mM acetate. mESCs cultured with LIF serve as negative control.

(F) Cell numbers were not affected by the addition of acetate to I3 cell media, similar to all tested lines.

(G) Immunofluorescence analysis shows acetate significantly delayed ($p < 0.001$) Sox17 expression following 48 hr of endoderm induction (Activin + Wnt3A) in H1 hESCs grown on Matrigel. H1 cells cultured in mTeSR provide a negative control.

(H) FACS analysis of H1 hESCs expressing *OCT4-GFP* shows that delayed addition of acetate, 24 and 48 hr post-differentiation, can similarly block loss of OCT4 expression.

(I) FACS analysis of H1 hESCs expressing *OCT4-GFP* maintained for 5 days with bFGF and acetate shows higher OCT4 expression than those cultured on bFGF alone. Naive cells grown in mTeSR provide negative controls for (C), (D), (H), and (I).

(J and K) FACS analyses of H1 hESCs expressing *OCT4-GFP* and stained with Tra-1-81. Left vertical axis and red bars represent the percentage of cells, which are positive for both pluripotency markers. Right vertical axis and blue bars represent the percentage of cells, which are negative for both pluripotency markers. The retention of the expression of OCT4 and Tra-1-81 by acetate is dose-dependent. In all histograms, unlabeled cells and isotype controls are represented in gray. Error bars represent standard deviation. *$p \leq 0.05$; **$p \leq 0.01$; ***$p \leq 0.001$.

et al., 2012; Ware et al., 2009). Ac-CoA is a substrate of acetylation, suggesting that acetate level might affect the histone acetylation state of hESCs. To test this hypothesis, we stained hESC colonies after 24 hr of spontaneous differentiation against H3K9/K27ac, a well-known pan-acetylation marker, and H3K27 methylation. Differentiating cells lost H3K9/K27 acetylation at the edges of the colony, while pluripotent cells did not (Figures 4A and 4B). The addition of acetate blocked the H3K9/K27 acetylation loss. H3K27 methylation was unaffected in all conditions. We repeated the staining of hESCs after 24 hr of spontaneous differentiation with H3 and H4 pan-acetylation antibodies, with similar results (Figures 4C and 4D). The addition

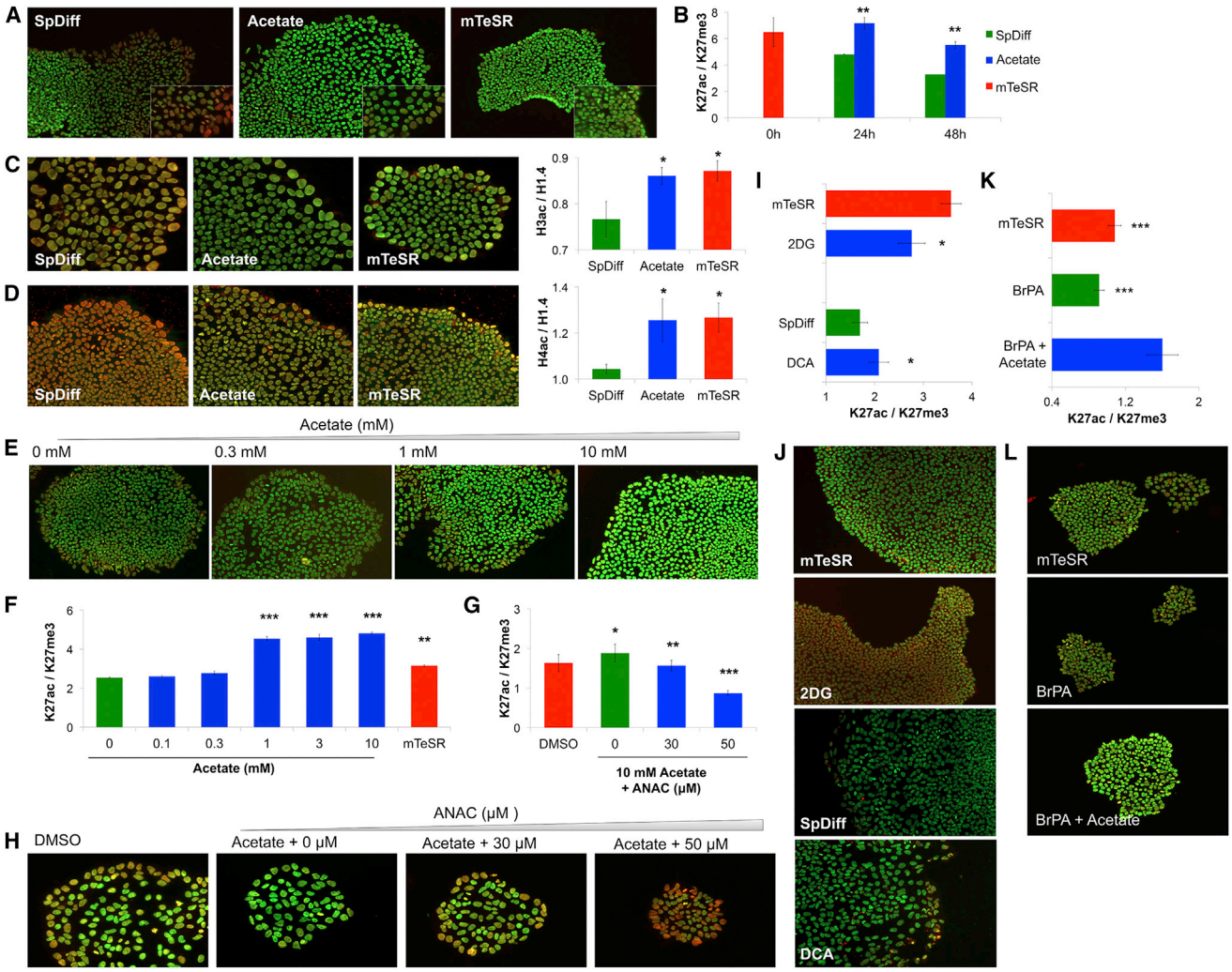

Figure 4. Acetate Induces Histone Pan-Acetylation

(A and B) Immunofluorescence staining of H3K9/K27 acetylation (green) and H3K27me3 methylation (red) during early differentiation. (A) Spontaneous differentiation (SpDiff) causes loss of K9/K27ac acetylation in the circumference of the colony at 24 hr. Addition of 10 mM acetate blocks this loss of histone acetylation. Untreated colonies in mTeSR serve as negative control. H3K27me3 methylation was not affected in all cases. (B) Kinetics of K9/K27 acetylation normalized to K27me3 shows that acetylation is primarily lost during the first 48 hr of differentiation, an effect that is inhibited by 10 mM acetate.

(C and D) Acetate also caused a significant increase in H3 and H4 acetylation, with no effect on H1.4 methylation.

(E–L) Immunofluorescence staining of H3K9/K27 acetylation (green) and H3K27me3 methylation (red) during early differentiation. (E and F) Acetate induces a dose-dependent increase of K9/K27 histone acetylation in hESCs in SpDiff. Acetylation is pronounced at concentrations above 0.3 mM. (G and H) Anacardic acid (ANAC), a histone acetyl transferase (HAT) inhibitor, abolished acetate-induced histone acetylation in a dose-dependent manner. (I and J) Immunofluorescence microscopy of I3 hESCs for K9/K27ac (green) and K27me3 (red) showed DCA (5 mM) significantly increased, while 2-DG (1.25 mM) significantly decreased histone acetylation after 24 hr. (K and L) BrPA (10 μM) significantly decreased histone acetylation after 24 hr. The addition of 10 mM acetate reversed this effect. Error bars represent standard errors. *$p \leq 0.05$; **$p \leq 0.01$; ***$p \leq 0.001$.

of acetate to cell medium blocked histone deacetylation above a concentration of 300 μM (Figures 4E and 4F). High doses of acetate induced hyper-acetylation ($p < 0.001$). Addition of anacardic acid (ANAC), a histone acetyltransferase inhibitor, abolished the acetylation of H3K9/K27 by acetate (Figures 4G and 4H).

Next, we sought to link the change in histone acetylation to the shift in glycolysis we identified in early differentiation. Indeed, inhibition of glycolysis by 2-DG or BrPA decreased H3K9/K27 acetylation in undifferentiated hESCs ($p < 0.05$ and $p < 0.001$, respectively) (Figures 4I–4L). This deacetylation was completely reversed by the addition of acetate ($p < 0.001$) (Figure 4L). Moreover, the addition of DCA, a PDK inhibitor that redirects pyruvate toward Ac-CoA, increased histone acetylation ($p < 0.05$) (Figures 4I and 4J). These results demonstrate that glycolytic production of Ac-CoA drives histone acetylation in pluripotent stem cells.

Metabolic Regulation of Ac-CoA Modulates ESC Pluripotency

The Warburg effect is thought to drive glucose toward lactate for the rapid production of ATP and nucleotides. The identification of

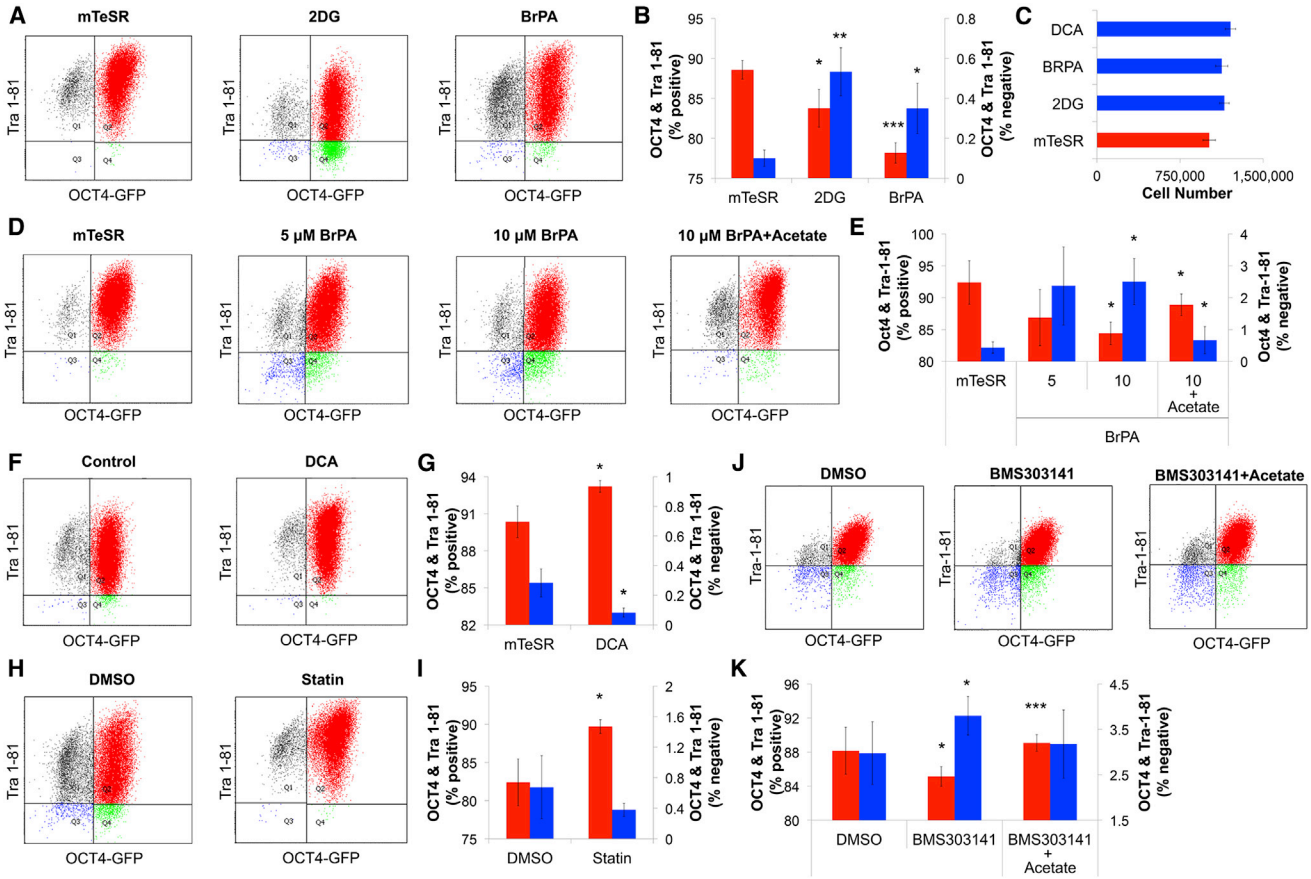

Figure 5. Glycolysis Regulates Stem Cell Pluripotency

(A–K) FACS analyses of H1 hESCs expressing *OCT4-GFP* and stained with Tra-1-81. Left vertical axis and red bars represent the percentage of cells, which are positive for both pluripotency markers. Right vertical axis and blue bars represent the percentage of cells, which are negative for both pluripotency markers. (A and B) Inhibition of glycolysis by 1.25 mM 2-DG or 10 μM BrPA significantly decreased the percentage of cells expressing both pluripotent markers, increasing the percentage of non-expressing cells. (C) H1 *OCT4-GFP* cell numbers are compared for treated versus non-treated cells. No significant effect of glycolytic inhibitors was noted on cell proliferation. (D and E) Four-day treatment of H1 hESCs with BrPA (5 or 10 μM) caused a dose-dependent loss in pluripotency markers. Acetate stimulation inhibited the downregulation of both markers. (F and G) Pyruvate dehydrogenase kinase (PDK) inhibitor DCA (5 mM) increased the percentage of cells positive for OCT4 and Tra-1-81 after 4 days of stimulation. (H and I) Inhibition of cholesterol synthesis in H1 hESCs by 10 μM lovastatin ("statin") similarly increased the percentage of cells positive for both pluripotency markers compared to the DMSO control. (J and K) BMS303141, an ACLY inhibitor, significantly decreased the percentage of both OCT4- and Tra-1-81-positive cells. Acetate added to cell media reversed this effect. Error bars represent standard deviation. *$p \leq 0.05$; **$p \leq 0.01$; ***$p \leq 0.001$.

a glycolytic induction of histone acetylation in pluripotent cells suggests that Ac-CoA production may be an essential factor in maintaining pluripotency. To examine the effect of Ac-CoA on pluripotency, we first blocked glycolysis in pluripotent cells upstream of pyruvate using 2-DG and BrPA. Four-day treatment with either inhibitor caused a significant loss in pluripotency markers OCT4 and Tra-1-81 ($p < 0.05$) (Figures 5A and 5B) without affecting cell proliferation (Figure 5C). This inhibition was reversed by the addition of acetate ($p < 0.05$) (Figures 5D and 5E). To further examine this pathway, we used DCA, a pyruvate dehydrogenase kinase (PDK) inhibitor that redirects pyruvate toward Ac-CoA. DCA was recently shown by Folmes and colleagues to block reprogramming to iPSCs (Folmes et al., 2011). However, in our system DCA redirection of pyruvate toward Ac-CoA significantly increased the percentage of pluripotent cells expressing OCT4 and Tra-1-81 ($p < 0.05$) (Figures 5F and 5G).

In addition to being a substrate for histone acetylation and oxidative phosphorylation, Ac-CoA can also be used to synthesize cholesterol. Indeed, pluripotent cells synthesized cholesterol when grown in mTeSR culture medium (Figure 2D). To block cholesterol synthesis from Ac-CoA, we used lovastatin, an HMG-CoA reductase inhibitor, and observed an increase in $OCT4^{+}$ + $Tra\text{-}1\text{-}81^{+}$ pluripotent cells ($p < 0.05$), similar to DCA treatment (Figures 5H and 5I).

Finally, our gene expression and proteomic analyses point to a 5- and 2-fold decrease, upon pluripotent stem cell differentiation, in *ACLY*, a major enzyme responsible for production of Ac-CoA for histone acetylation (Figure 2H; Figure S2A) (Wellen et al., 2009). To show ACLY involvement, we used BMS303141, a specific ACLY inhibitor. BMS303141 significantly decreased the expression of pluripotency markers, and this effect was completely reversed by the addition of acetate (Figures 5J and 5K). To exclude a possible apoptotic effect of the different

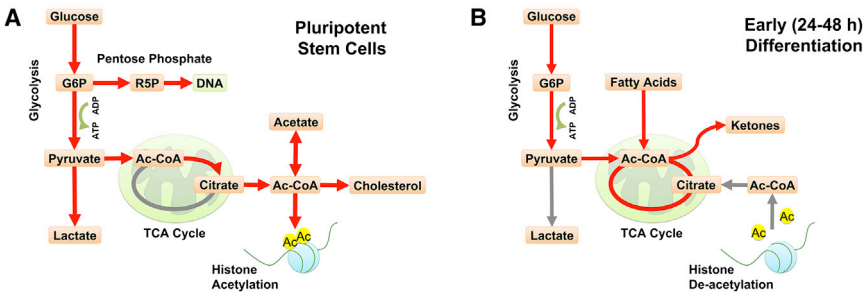

Figure 6. Metabolic Regulation of Histone Acetylation in Pluripotent Cells and Early Differentiation

(A) Glycolysis in pluripotent cells is increased, resulting in increased levels of Ac-CoA and histone acetylation.

(B) Upon early differentiation, Ac-CoA is consumed in the TCA cycle, yielding less histone acetylation.

inhibitors used, a TUNEL assay was performed, with no effect seen for any of the inhibitors used at the specified concentrations for 4 days (Figures S2B and S2C). Modulation of fatty acid oxidation did not affect pluripotency (Figures S3D and S3E).

Altogether, our results show that redirection of metabolic flux away from Ac-CoA is a critical factor mediating the loss of pluripotency.

DISCUSSION

Differentiation of pluripotent stem cells is a complex phenomenon regulated on multiple levels. In this work we focused on the earliest events that accompany the gradual loss of pluripotent potential, a time point that is poorly understood (Dejosez and Zwaka, 2012; Drukker et al., 2012).

To the best of our knowledge, the metabolites identified in the current study construct the first metabolic profile of early-differentiating cells as well as the first study of the metabolome of PSCs in suspension. Our findings show that aerobic glycolysis plays a critical role in maintaining histone acetylation, associated with the open chromatin structure of PSCs. We show that this glycolytic switch turns off during the first 24 hr of differentiation, leading to Ac-CoA deprivation-mediated loss of histone acetylation and pluripotency markers. These findings mark the earliest metabolic switch identified to date, linking the Warburg effect with epigenetic regulation of pluripotent stem cells (Figure 6).

The Warburg effect, defined by the fermentation of glucose to lactate (Metallo and Vander Heiden, 2013), was first described in cancer cells by Nobel laureate Otto Heinrich Warburg in 1924 and more recently reported in embryonic and induced pluripotent stem cells (Folmes et al., 2011; Panopoulos et al., 2012; Zhu et al., 2010). Recent work comparing PSCs to terminally differentiated cells showed low levels of oxidative phosphorylation in PSCs and increased aerobic glycolysis due to inactivation of pyruvate dehydrogenase (PDH) (Varum et al., 2011) or the expression of uncoupling protein 2 (UCP2) (Zhang et al., 2011). In contrast, our results, tracking the first steps of differentiation, show a similar loss of glycolysis, minor difference in *UCP2* expression, and an actual increase in *PDHB* (Figures 2E–2H), suggesting that a different mechanism might be responsible for the lack of oxidative phosphorylation in pluripotent cells.

This increase in glycolysis is known to generate ATP at a faster rate than oxidative phosphorylation, with lower ROS production, important features for rapidly proliferating cells (Xu et al., 2013). Glycolysis also shunts into the pentose phosphate pathway, producing much-needed nucleotides for proliferation (Vander Heiden et al., 2009). However, these advantages do not explain the increased conversion of glucose to Ac-CoA, which we observed using high-resolution NMR and ^{13}C glucose tracing using mass spectrometry (Figures 1 and 2G; Figure S1). Aerobic glycolysis is thought to direct pyruvate toward lactate rather than Ac-CoA (Vander Heiden et al., 2009). In fact, inhibiting PDK in cancer cells redirects pyruvate from lactate to Ac-CoA and oxidative phosphorylation, effectively killing the cells (Pearson, 2007). Surprisingly, the same redirection from lactate to Ac-CoA actually increases pluripotency in hESCs (Figure 5F) without affecting their viability. These results suggest an underlying metabolic difference between cancer cells and PSCs, but also stand in contrast to the findings of Folmes and colleagues (Folmes et al., 2011). Folmes and his co-workers showed that acetate production increased during reprogramming of mouse cells to iPSC. This observation may be explained by the change in Ac-CoA levels, as Ac-CoA, the active entity, is in equilibrium with acetate. As Ac-CoA is not normally secreted from cells, acetate may serve as a form of paracrine signaling designed to support the pluripotent state of next-door neighbors in the colony. However, treatment with DCA blocked reprogramming to iPSC. Together with the results shown here and previous studies on cancer cell metabolism (Vander Heiden et al., 2009), these results may suggest that oxidative phosphorylation is inactive in the pluripotent state, allowing the cells to push pyruvate to Ac-CoA through overexpression of ACLY. However, cancer cells and somatic cells undergoing reprogramming actively seek to avoid a functional TCA cycle. In that case, DCA treatment reignites oxidative phosphorylation, reducing reprogramming efficiency or outright killing cancer cells.

Interestingly, despite the key role suggested for fatty acids in mouse ESC differentiation (Yanes et al., 2010) and energy generation, our data suggest that lipid metabolism plays a minor role in early differentiation. We show that Ac-CoA utilization in cholesterol biosynthesis negatively effects pluripotency. However, fatty acid oxidation is minor, and its modulation using lipids and pharmaceutical agents showed no effect on the expression of pluripotency markers (Figures S3D and S3E).

In summary, our work reveals a crucial role for glycolysis in the maintenance of the pluripotent state. We show that human and mouse ESCs direct pyruvate toward Ac-CoA and histone acetylation. Blocking Ac-CoA production causes loss of pluripotency, while preventing its consumption through pharmaceutical or metabolic modulation can significantly delay the differentiation of the cells. The results elucidate an important link between metabolism, pluripotency, and chromatin regulation and could be applied to optimize the culture of PSCs or removing teratoma-inducing cells from differentiated cultures.

Table 1. Multiple Reaction Monitoring (MRM) Transitions and Parameters for Ac-CoA and $^{13}C_2$-Ac-CoA

Name	Q1 *m/z*	Q3 *m/z*	DP V	EP V	CXP V	CE eV
Ac-CoA 1 (quantifier transition)	808.1	78.9	−50	−10	−7	−126
Ac-CoA 2 (qualifier transition)	403.5	78.9	−35	−10	−19	−112
$^{13}C_2$-Ac-CoA 1 (quantifier transition)	810.1	78.9	−50	−10	−7	−126
$^{13}C_2$-Ac-CoA 2 (qualifier transition)	404.8	78.9	−35	−10	−19	−112

Calibration samples of Ac-CoA (0.1–2 μM) were prepared in water and cell extracts according to the standard addition method. Q1, quadrupole 1; *m/z*, mass-to-charge ratio; Q3, quadrupole 3; DP, declustering potential; V, volts; EP, entrance potential; CXP, collision cell exit potential; CE, collision energy; eV, electronvolts.

EXPERIMENTAL PROCEDURES

hESC Culture

hESC lines I3 and I4 were maintained as previously described (Amit et al., 2011). WA01 (H1) and H1 *OCT4-eGFP* were purchased from the WiCell Research Institute. Cells were maintained in StemCell Technologies mTeSR1 culture medium on Matrigel-coated plates and passaged every 4–7 days using dispase II (Roche).

mESC Culture

R1 *OCT4-GFP* line was a kind gift of Prof. Andras Nagy of the Lunenfeld Research Institute. Briefly, mESCs were maintained in DMEM supplemented with 15% FBS, sodium pyruvate, L-glutamine, β-mercaptoethanol, and 1,000 U/ml murine leukemia inhibitory factor (LIF). Cells were passaged every 2–3 days using trypsin EDTA.

High-Density Suspension Cultures

To produce a large number of cells for metabolic studies, I3 and I4 hESC lines were cultured in high-density suspension as previously described (Amit et al., 2011). Briefly, hESCs were removed from culture dishes using collagenase IV, broken into clumps using a pipette, and transferred to a low-adhesion 60 mm dish at a density of 3 × 10^6 cells/ml. After three passages of adaptation to suspension, cells were transferred to 100 ml spinner flasks stirred at 75 rpm. Cultures were maintained in suspension medium (SM10F) culture medium composed of DMEM/F12 supplemented with 15% KO serum, L-glutamine, β-mercaptoethanol, 10 ng/ml bFGF, and 100 pg/ml of IL6RIL6 chimera. Spontaneous differentiation was carried out in suspension by removing bFGF and IL6RIL6 chimera from the culture medium, minimizing culture and medium artifacts.

Sample Preparation for NMR Analysis

I3 and I4 hESCs were collected from spinners, spun down, and washed with PBS. Samples of 5 × 10^6 cells were snap-frozen in liquid nitrogen and stored at −80°C for subsequent analysis. Samples were thawed and quenched in 60% MeOH, ultrasonicated at 4°C, and lyophilized. Lyophilized samples were resuspended in ice-cold methanol/chloroform (2:1), homogenized for 5 min, and finally mixed with a volume of chloroform/water (1:1). Phase separation was carried out by 20 min centrifugation at 1,500 *g* at 4°C. Top aqueous and bottom organic layers were transferred to clean tubes. Middle protein ring was re-extracted by repeating the process and samples were pooled. Tubes were finally dried in SpeedVac and stored at −80°C until analysis. Medium samples were collected from culture density of 1 × 10^6 cells/ml, centrifuged to remove cells and debris, and stored at −80°C until analysis. Sample volume was adjusted according to protein concentration.

NMR Analysis

High-resolution NMR analysis was carried out at the CNRS (Lyon, France). ^{1}H-NMR spectra were recorded on a Bruker Avance III spectrometer operated at 800.15 MHz (^{1}H resonance frequency; 18.8 T), equipped with a 5 mm TXI probehead and refrigerated high-throughput sample changer. The temperature was regulated at 300 K throughout the experiments. Frozen samples were reconstituted in D_2O phosphate buffer solution (pH 7.2) containing 0.1 mM and 1 mM TSP (3-(trimethylsilyl)propionate-2,2,3,3-d4) for cell extracts and media samples, respectively. For each sample, ^{1}H 1D NOESY and CPMG experiments (media), or ^{1}H 1D NOESY alone (cell extracts) were acquired with presaturation of the water signal. All free induction decays (FIDs) were multiplied by an exponential function corresponding to a 0.3 Hz line-broadening factor prior to Fourier transform. Phase and baseline of the spectra were manually adjusted in TopSpin 3.1 (Bruker Biospin GmbH). Spectra were calibrated on the α-glucose doublet at δ = 5.23 ppm or the TSP signal at δ = −0.016 ppm for the cell aqueous extracts or the media samples respectively, and reduced over the chemical shift range 0.1–10 ppm to 9,900 bins (10^{-3} ppm wide) with integration of signal intensity using the AMIX software (Bruker GmbH). Residual water signal (δ = 4.65–4.9 ppm) was discarded prior to further analysis.

Untargeted Metabolomics Data Analysis

NMR spectral bins were analyzed using MetaboAnalyst 2.0 (Xia et al., 2009). Data were filtered by interquantile range and normalized to the sum. Following PCA and random forest outlier detection, two samples were excluded from the I4 media dataset. PLS regression was performed using the PLSR function. Classification and cross-validation were performed using the corresponding wrapper function offered by the caret package. In order to assess if the class discrimination is statistically significant, a permutation test was performed. In each permutation, a PLS-DA model was built between the data (X) and the class labels (Y) using the optimal number of components, determined by cross validation for the model based on the original class assignment. The ratio of the between sum of the squares and the within sum of squares for the class assignment prediction of each model was calculated. Hierarchical clustering was performed using Spearman correlation and the Ward clustering algorithm. Metabolite identification was performed using Chenomx NMR suite 7.7 (Chenomx Inc.).

Mass Spectrometry for ^{13}C-Ac-CoA

I3 hESCs were maintained for 48 hr in SpDiff or mTeSR media. Following 8 hr of incubation with D-glucose-$^{13}C_6$, cells were scraped in cold 80% MeOH, snap frozen in liquid nitrogen, and transferred to −80°C until analysis. Cell pellets were thawed on ice and ultrasonicated at 4°C. Samples were then centrifuged at 4°C, and supernatant was transferred to clean tubes. Pellets were left for protein quantification. Samples were dried in SpeedVac and reconstituted in HPLC-grade water. The chromatography was performed using a Shimadzu UHPLC System, series Nexera. The chromatographic separations were performed on a Kinetex (Phenomenex) column (C18, 2.6 μm particle size, 100 Å pore size, 50 × 2.1 mm). The injection volume was 20 μl, the oven temperature was maintained at 40°C, and the autosampler tray temperature was maintained at 15°C. Chromatographic separation was achieved using a linear gradient program at a constant flow rate of 0.35 ml/min over a total run time of 6 min from 99% to 60% solvent A. Solvent A was 20 mM ammonium acetate and 20 mM ammonium hydroxide (pH 9) in water and solvent B was 20 mM ammonium acetate in methanol. Water was used for washing the needle prior to each injection cycle. All samples were analyzed in duplicate. Ac-CoA was detected by an AB Sciex Triple Quad 5500 mass spectrometer in negative ion mode using electrospray ionization (ESI) and multiple-reaction monitoring (MRM) mode of acquisition. The ions $[Ac\text{-}CoA\text{-}H]^-$ (*m/z* 808.1) and $[Ac\text{-}CoA\text{-}2H]^{2-}$ (*m/z* 403.5) were selected in the first mass analyzer and fragmented in the collision cell followed by detection of the products of fragmentation in the second mass analyzer. Two transitions were monitored: *m/z* 808.1 → 78.9 (quantifier) and *m/z* 403.5 → 78.9 (qualifier). The TurboIonspray probe temperature was set at 650°C with the ionization potential at −4,500 V. Data acquisition and analysis were performed on a Dell OptiPlex 960 computer with Analyst 1.6 software distributed by AB Sciex (Table 1).

Proteome Analysis

Proteome analysis was performed as described by us previously (Liu et al., 2012). Briefly: to achieve quantitative proteome data, a "heavy" proteome reference was spiked in equal amounts in every sample. Harvested cells were lysed in an appropriate amount of urea buffer (8M urea, 50 mM Tris-HCl

[pH 7.4]). The lysates were cleared by centrifugation at 14,000 rpm for 15 min at 4°C. Disulfide bridges were then reduced in DTT 2 mM for 30 min at 25°C, and successively free cysteines were alkylated in 11 mM iodoacetamide for 20 min at room temperature in the darkness. LysC digestion was performed by adding LysC (Wako) in a ratio of 1:40 (w/w) to the sample and incubating it for 18 hr under gentle shaking at 30°C. After LysC digestion, the samples were diluted three times with 50 mM ammonium bicarbonate solution, immobilized trypsin (Applied Biosystems) was added, and samples were incubated for 4 hr under rotation at 30°C. Digestion was stopped by acidification with trifluoroacetic acid and removal of trypsin beads by centrifugation. After digestion, peptides were extracted and desalted before analysis by mass spectrometry. Five microliters were injected in duplicate on a LC-MS/MS system (Agilent 1200 [Agilent Technologies] and LTQ-Orbitrap Velos [Thermo]), using a 240 min gradient from 5% to 40% of solvent B (80% acetonitrile, 0.1% formic acid; solvent A 5% acetonitrile, 0.1% formic acid). For the chromatographic separation, a 20 cm capillary (75 mm inner diameter) was packed with 3 mm C18 beads (ReproSil-Pur C18 AQ, Dr. Maisch). On one end of the capillary, a nanospray tip was generated using a laser puller (P-2000 Laser Based Micropipette Puller, Sutter Instruments), allowing fretless packing. Then a nanospray source was operated with a spray voltage of 1.9 kV and an ion transfer tube temperature of 260°C. Data were acquired in data-dependent mode, with one survey MS scan in the Orbitrap mass analyzer followed by up to 20 MS/MS scans in the ion trap on the most intense ions (intensity threshold, 500 counts). Once selected for fragmentation, ions were excluded from further selection for 30 s to increase new sequencing vents. Proteome raw data were analyzed using the MaxQuant proteomics pipeline (v.1.1.1.36) and the built-in Andromeda search engine with the International Protein Index Mouse database. Carbamidomethylation of cysteines was chosen as fixed modification, and oxidation of methionine and acetylation of N terminus were chosen as variable modifications. The search engine peptide assignments were filtered at 1% FDR and the feature match between runs was not enabled; second peptide feature was enabled, while other parameters were left as default. Two ratio counts were set as threshold for quantification. Gene Ontology analysis was performed using a DAVID tool.

Early Endoderm Induction

Cells were cultured for 48 hr in RPMI medium supplemented with B27, 100 ng/ml activin A, and 50 ng/ml Wnt3A. Media were changed after 24 hr, and the cells were fixed for analysis.

Flow Cytometry

Flow cytometry was carried out on Becton Dickinson FACSAria III. Cells were washed in PBS, dissociated using TrypLE select (Invitrogen), and centrifuged at 300 *g* for 5 min. Cell pellets were resuspended in PBS containing 1% FBS, filtered through a cell strainer to remove aggregates, and incubated with primary conjugated antibodies for 1 hr on ice. Cells were then washed twice, suspended in PBS with 1% FBS, and analyzed. Live, single cells were gated by GFP, PE, or side-scatter emission. Unlabeled cells and isotype controls were used to set gates for negative populations. Data analysis was performed using TreeStar Inc. FlowJo software.

Immunofluorescence Microscopy

Cultures were washed twice with PBS and fixed with 4% paraformaldehyde for 15 min at room temperature. Cells were permeabilized with 0.5% Triton X-100 for 5 min and blocked with 1% BSA for 1 hr. Cells were incubated with primary antibodies for 1 hr, then washed and incubated with secondary antibodies for 1 hr at room temperature. Samples were imaged on a Zeiss LSM 700 microscope. Images were analyzed using the ZEN 2011 software, as well as the Broad Institute Cell Profiler image analysis software.

Antibodies

Primary PE-conjugated antibodies used for FACS analyses included anti-Tra-1-60 and Tra-1-81 (1:20; eBioscience) as well as anti-SSEA4 (1:50; R&D Systems). Anti-H3K9/K27ac was a kind gift of Prof. H. Kimura of Osaka University. Additional antibodies used include anti-H3K27me3 (1:1,000; EMD Millipore), anti-H3ac (1:200; EMD Millipore), anti-H4ac (1:100; EMD Millipore), anti-H1.4 (1:200; EMD Millipore), and anti-SOX17 (1:100; R&D Systems). Secondary antibodies were purchased from Jackson Immunoresearch Laboratories.

Quantitative Gene Expression Analysis

Total cellular RNA was extracted using Life Technologies TRIzol reagent and reversed transcribed using Promega ImProm-II kit according to manufacturer directions. Real-time PCR was performed using Applied Biosystem Power SYBR Green PCR Master Mix and analyzed on the company's 7300 real-time PCR system (Table S1).

TUNEL Assay

Quantitation of apoptotic cells was performed utilizing DeadEnd Fluorometric TUNEL System (Promega) according to manufacturer directions. Briefly, cells were permeabilized and exposed to fluorescein-12-dUTP and terminal deoxynucleotidyl transferase (TdT), dying apoptotic nuclei green. The reaction was subsequently stopped and the cells counterstained for DAPI. A percent apoptotic nucleus was calculated by dividing the number of TUNEL- to DAPI-positive nuclei.

Drugs and Reagents

Drugs and reagents were purchased from Sigma-Aldrich unless otherwise indicated. 2-DG, BrPA, and DCA were purchased from Santa Cruz Biotechnology. Lovastatin was purchased from Cayman Chemical. BMS 303141 was purchased from Tocris Bioscience. Ac-CoA standard was used from a Biovision kit (see Metabolic Kits, below).

Metabolic Kits

Glucose and lactate levels were determined using commercial kits based on glucose oxidase (Stanbio Laboratory) and lactate oxidase (Trinity Biotech Bray), respectively. Ac-CoA, free fatty acids, and cholesterol were quantified by CoA derivatives and cholesterol oxidase, respectively, using commercial kits purchased from BioVision. Ketone bodies were determined by NADH disappearance using a commercial kit purchased from Abnova. All targeted metabolic assays were performed according to manufacturer's instructions.

SUPPLEMENTAL INFORMATION

Supplemental Information includes three figures and one table and can be found with this article online at http://dx.doi.org/10.1016/j.cmet.2015.02.002.

ACKNOWLEDGMENTS

We thank Prof. Nissim Benvenisty, Prof. Ruby Shalom-Feuerstein, Dr. Isabelle Petit, and Dr. Michael Shmoish for important discussions, as well as Eayar Leibovitch, SabinaTsytkin, and Chaya Rachel Calderon for technical support. This work was supported by a European Research Council Starting Grant TMIHCV (no. 242699), Marie Curie International Reintegration Grant microLiverMaturation (no. 248417), the British Council BIRAX Regenerative Medicine award (no. 33BX12HGYN), Agence Nationale pour la Recherche GENOPAT-08 (no. ANR-08-GENO-024), and a Très grandes infrastructures de recherche (TGIR-RMN-THC CNRS FR3050). A.M. was partly supported by an INSERM postdoctoral fellowship.

Received: May 5, 2014
Revised: November 16, 2014
Accepted: February 6, 2015
Published: March 3, 2015

REFERENCES

Amit, M., Laevsky, I., Miropolsky, Y., Shariki, K., Peri, M., and Itskovitz-Eldor, J. (2011). Dynamic suspension culture for scalable expansion of undifferentiated human pluripotent stem cells. Nat. Protoc. *6*, 572–579.

Blair, K., Wray, J., and Smith, A. (2011). The liberation of embryonic stem cells. PLoS Genet. *7*, e1002019.

Cezar, G.G., Quam, J.A., Smith, A.M., Rosa, G.J., Piekarczyk, M.S., Brown, J.F., Gage, F.H., and Muotri, A.R. (2007). Identification of small molecules from human embryonic stem cells using metabolomics. Stem Cells Dev. *16*, 869–882.

Dejosez, M., and Zwaka, T.P. (2012). Pluripotency and nuclear reprogramming. Annu. Rev. Biochem. *81*, 737–765.

Drukker, M., Tang, C., Ardehali, R., Rinkevich, Y., Seita, J., Lee, A.S., Mosley, A.R., Weissman, I.L., and Soen, Y. (2012). Isolation of primitive endoderm, mesoderm, vascular endothelial and trophoblast progenitors from human pluripotent stem cells. Nat. Biotechnol. *30*, 531–542.

Folmes, C.D., Nelson, T.J., Martinez-Fernandez, A., Arrell, D.K., Lindor, J.Z., Dzeja, P.P., Ikeda, Y., Perez-Terzic, C., and Terzic, A. (2011). Somatic oxidative bioenergetics transitions into pluripotency-dependent glycolysis to facilitate nuclear reprogramming. Cell Metab. *14*, 264–271.

Hezroni, H., Tzchori, I., Davidi, A., Mattout, A., Biran, A., Nissim-Rafinia, M., Westphal, H., and Meshorer, E. (2011). H3K9 histone acetylation predicts pluripotency and reprogramming capacity of ES cells. Nucleus *2*, 300–309.

Liu, L., Ulbrich, J., Müller, J., Wüstefeld, T., Aeberhard, L., Kress, T.R., Muthalagu, N., Rycak, L., Rudalska, R., Moll, R., et al. (2012). Deregulated MYC expression induces dependence upon AMPK-related kinase 5. Nature *483*, 608–612.

Meissen, J.K., Yuen, B.T., Kind, T., Riggs, J.W., Barupal, D.K., Knoepfler, P.S., and Fiehn, O. (2012). Induced pluripotent stem cells show metabolomic differences to embryonic stem cells in polyunsaturated phosphatidylcholines and primary metabolism. PLoS ONE *7*, e46770.

Melcer, S., Hezroni, H., Rand, E., Nissim-Rafinia, M., Skoultchi, A., Stewart, C.L., Bustin, M., and Meshorer, E. (2012). Histone modifications and lamin A regulate chromatin protein dynamics in early embryonic stem cell differentiation. Nat. Commun. *3*, 910.

Metallo, C.M., and Vander Heiden, M.G. (2013). Understanding metabolic regulation and its influence on cell physiology. Mol. Cell *49*, 388–398.

Panopoulos, A.D., Yanes, O., Ruiz, S., Kida, Y.S., Diep, D., Tautenhahn, R., Herrerías, A., Batchelder, E.M., Plongthongkum, N., Lutz, M., et al. (2012). The metabolome of induced pluripotent stem cells reveals metabolic changes occurring in somatic cell reprogramming. Cell Res. *22*, 168–177.

Pearson, H. (2007). Cancer patients opt for unapproved drug. Nature *446*, 474–475.

Shyh-Chang, N., Locasale, J.W., Lyssiotis, C.A., Zheng, Y., Teo, R.Y., Ratanasirintrawoot, S., Zhang, J., Onder, T., Unternaehrer, J.J., Zhu, H., et al. (2013). Influence of threonine metabolism on S-adenosylmethionine and histone methylation. Science *339*, 222–226.

Vander Heiden, M.G., Cantley, L.C., and Thompson, C.B. (2009). Understanding the Warburg effect: the metabolic requirements of cell proliferation. Science *324*, 1029–1033.

Varum, S., Rodrigues, A.S., Moura, M.B., Momcilovic, O., Easley, C.A., 4th, Ramalho-Santos, J., Van Houten, B., and Schatten, G. (2011). Energy metabolism in human pluripotent stem cells and their differentiated counterparts. PLoS ONE *6*, e20914.

Ware, C.B., Wang, L., Mecham, B.H., Shen, L., Nelson, A.M., Bar, M., Lamba, D.A., Dauphin, D.S., Buckingham, B., Askari, B., et al. (2009). Histone deacetylase inhibition elicits an evolutionarily conserved self-renewal program in embryonic stem cells. Cell Stem Cell *4*, 359–369.

Wellen, K.E., Hatzivassiliou, G., Sachdeva, U.M., Bui, T.V., Cross, J.R., and Thompson, C.B. (2009). ATP-citrate lyase links cellular metabolism to histone acetylation. Science *324*, 1076–1080.

Xia, J., Psychogios, N., Young, N., and Wishart, D.S. (2009). MetaboAnalyst: a web server for metabolomic data analysis and interpretation. Nucleic Acids Res. *37*, W652–W660.

Xu, H.N., Zheng, G., Tchou, J., Nioka, S., and Li, L.Z. (2013). Characterizing the metabolic heterogeneity in human breast cancer xenografts by 3D high resolution fluorescence imaging. Springerplus *2*, 73.

Yanes, O., Clark, J., Wong, D.M., Patti, G.J., Sánchez-Ruiz, A., Benton, H.P., Trauger, S.A., Desponts, C., Ding, S., and Siuzdak, G. (2010). Metabolic oxidation regulates embryonic stem cell differentiation. Nat. Chem. Biol. *6*, 411–417.

Zhang, J., Khvorostov, I., Hong, J.S., Oktay, Y., Vergnes, L., Nuebel, E., Wahjudi, P.N., Setoguchi, K., Wang, G., Do, A., et al. (2011). UCP2 regulates energy metabolism and differentiation potential of human pluripotent stem cells. EMBO J. *30*, 4860–4873.

Zhu, S., Li, W., Zhou, H., Wei, W., Ambasudhan, R., Lin, T., Kim, J., Zhang, K., and Ding, S. (2010). Reprogramming of human primary somatic cells by OCT4 and chemical compounds. Cell Stem Cell *7*, 651–655.

Cell Metabolism

Supplemental Information

Glycolysis-Mediated Changes in Acetyl-CoA and Histone Acetylation Control the Early Differentiation of Embryonic Stem Cells

Arieh Moussaieff, Matthieu Rouleau, Daniel Kitsberg, Merav Cohen, Gahl Levy, Dinorah Barasch, Alina Nemirovski, Shai Shen-Orr, Ilana Laevsky, Michal Amit, David Bomze, Bénédicte Elena-Herrmann, Tali Scherf, Malka Nissim-Rafinia, Stefan Kempa, Joseph Itskovitz-Eldor, Eran Meshorer, Daniel Aberdam, and Yaakov Nahmias

SUPPLEMENT FIGURES

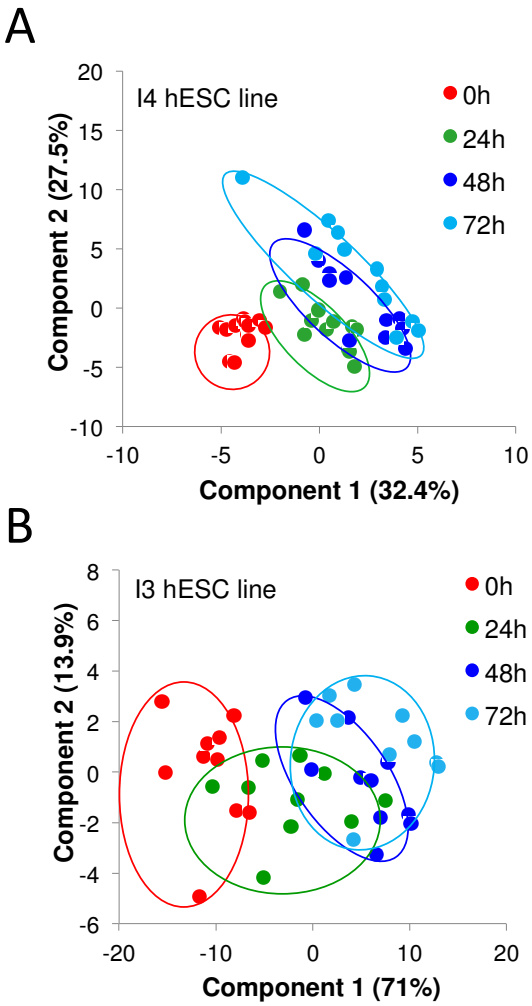

C

Metabolite	I4 Extract			I3 Medium				I4 Medium				Spectra	
	0h	24h	48h	0h	24h	48h	72h	0h	24h	48h	72h	Shift*	Multiplicity
Lactate												4.1	q
Acetate												1.9	s
β-glucose												4.6	d
α-glucose												5.2	d
Maltose												5.4	d
$							$						$
Citrate												2.5	d
Ornithine												3	t
Ascorbate												4.5	d
							$						
Asparagine												2.85	m
Aspartate												2.8	dd
Citrulline												1.6	m
Cystine												3.4	dd
Glutamine												2.45	m
Glycine												3.55	s
Histidine												7.08	s
Hydroxyproline												4.3	m
Isoleucine												1	d
Leucine												0.95	dd
Lysine												3.02	t
Methionine												2.64	t
Phenylalanine												7.32	d
Proline												3.33	m
Serine												3.94	m
Threonine												4.24	m
Tryptophan												7.73	d
Tyrosine												7.18	d
Valine												3.6	d
$											$		$
Formate												8.44	s
2-Phenylpropionate												1.4	d
Choline												3.2	s
Ethanol												1.17	t
							$						
Succinate							$					2.4	s
Alanine							$					1.5	d
myo-inositol							%0.5$					3.5	dd
Betaine												3.3	s
Glutathione												2.9	m
Cystathionine												2.7	m
Glutamate*							%1$					3.8	dd
ADP+ATP												8.3	s
NAD+							%5$					8.2	dd
UDP-X							$$					7.9	d
GTP												5.9	d
GPC							$					3.2	s
O-phospho choline							$					3.2	s

Figure S1, *related to Figure 1*. **Metabolic profile of hESC changes during early differentiation.** A-B) PLS-DA plots of ^{1}H NMR spectral bins of I4 and I3 hESC lines shows significant changes after 24-48 hours of differentiation (p≤0.001for I4 and p≤0.01 for I3; n=10-12), and a clear gradient of metabolic change over the first 72 hours. C) High resolution NMR analysis identified 44 metabolites in I4 and I3 cells and medium samples.

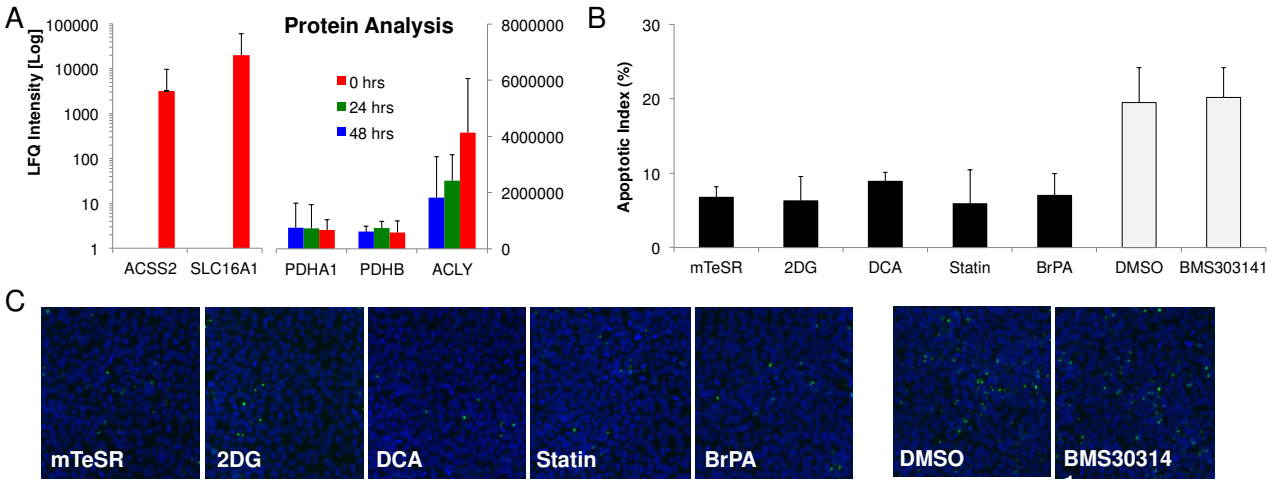

Figure S2, *related to Figure 2*. **Proteome and metabolic analysis of H1 hESC**. A) Proteome analysis of H1 hESCs shows the inhibition of SLC16A1 monocarboxylate transporter as well as ACSS and ACLY enzymes responsible for Ac-CoA cytosolic production and conversion to acetate. B-C) Metabolic pathways were dissected using inhibitor concentrations that showed minimal effect on cell viability evaluated by TUNEL staining for apoptosis. Error bars represent standard deviation.

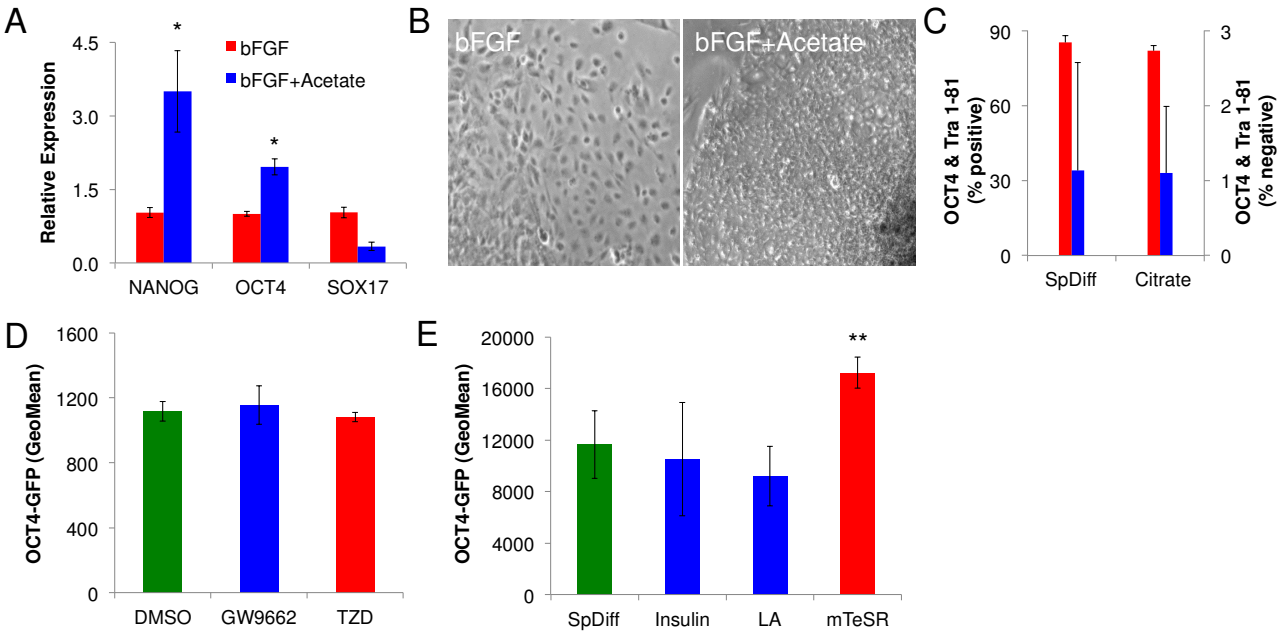

Figure S3, *related to Figure 3*. **Metabolic modulation of Ac-CoA affects hESC differentiation.** A-B) hESC maintained for 8 passages with bFGF but without feeder cells show a loss of pluripotent morphology. The addition of acetate increased the expression of OCT4 and NANOG by 3 and 2-fold, respectively ($p \leq 0.05$), while decreasing the expression of SOX17 by 3 folds ($p \leq 0.05$). Cellular morphology was similarly maintained. C) The addition of 1 mM citrate did not change the expression of OCT4 and Tra-1-81 during early differentiation. Red bars mark the percentage of cells positive for both pluripotency markers, while blue bars mark the cells, negative for both pluripotency markers. Error bars represent standard errors. D) PPAR inhibitor GW9662 and agonist thiazolidinedione (TZD) showed no effect on the expression of OCT4 compared to DMSO control. E) The addition of linoleic acid (LA) or insulin during early differentiation did not affect expression of OCT4-GFP. Error bars represent standard deviation. *, $p \leq 0.05$; **, $p \leq 0.01$

Table S1. qRT-PCR Primers

Gene	Forward	Reverse
RPL32	CTCTTTCCACGATGGCTTTG	GTCAAGGAGCTGGAAGTGCT
OCT4	TGGGCTCGAGAAGGATGTG	GCATAGTCGCTGCTTGATCG
SOX17	GGCGCAGCAGAATCCAGA	CCACGACTTGCCCAGCAT
NANOG	CCTGTGATTTGTGGGCCTG	GACAGTCTCCGTGAGGCAT
PAX6	TCCTTCTCGCTGGCTGTAAT	CCTGGAGCTCTGTTTGGAA
Brachyury	CAACCTCACTGACGGTGAAAAA	ACAAATTCTGGTGTGCCAAAGTT
GATA4	TAGACCGTGGGTTTTGCATTG	CATCCAGGTACATGGCAAACAG
REX1	ACCAGCACACTAGGCAAACC	TTCTGTTCACACAGGCTCCA
ACLY	CATATCCAGAGGAAGCCTACATTG	ATG GTC CAG ATC CTC CCT TT
PDHB	GTATGGATGAGGAGCTGGAAAG	GCCCTCGACTAACCTTGTATG
UCP2	GAACGGGACACCTTTAGAGAAG	CAGCAACAAGACGAGATAGAGG
ACSS2	TTGGGGCTTTGCACTCCATT	AGGCATCTGTAGTGATGAGAAGA
PDHA1	GTG TGA TGG GCA CCA TTC T	GGA CAG AGG CAA AGC TCA TT
PDK2	ATG AAA GAG ATC AAC CTG CTT CC	GGC TCT GGA CAT ACC AGC TC